

Calculation of induced current densities and specific absorption rates (SAR) for pregnant women exposed to hand-held metal detectors

Wolfgang Kainz, Dulciana D Chan, Jon P Casamento
and Howard I Bassen

Food and Drug Administration, Center for Devices and Radiological Health (CDRH),
12725 Twinbrook Parkway, Rockville, MD 20852, USA

E-mail: wxk@cdrh.fda.gov

Received 6 May 2003

Published 22 July 2003

Online at stacks.iop.org/PMB/48/2551

Abstract

The finite difference time domain (FDTD) method in combination with a well established frequency scaling method was used to calculate the internal fields and current densities induced in a simple model of a pregnant woman and her foetus, when exposed to hand-held metal detectors. The pregnant woman and foetus were modelled using a simple semi-heterogeneous model in 10 mm resolution, consisting of three different types of tissue. The model is based on the scanned shape of a pregnant woman in the 34th gestational week. Nine different representative models of hand-held metal detectors operating in the frequency range from 8 kHz to 2 MHz were evaluated. The metal detectors were placed directly on the abdomen of the computational model with a spacing of 1 cm. Both the induced current density and the specific absorption rate (SAR) are well below the recommended limits for exposure of the general public published in the ICNIRP Guidelines and the IEEE C95.1 Standard. The highest current density is 8.3 mA m^{-2} and the highest SAR is $26.5 \mu\text{W kg}^{-1}$. Compared to the limits for the induced current density recommended in the ICNIRP Guidelines, a minimum safety factor of 3 exists. Compared to the IEEE C95.1 Standard, a safety factor of 60 000 for the specific absorption rate was found. Based on the very low specific absorption rate and an induced current density below the recommended exposure limits, significant temperature rise or nerve stimulation in the pregnant woman or in the foetus can be excluded.

(Some figures in this article are in colour only in the electronic version)

1. Introduction

This paper investigates the exposure of pregnant women and their foetuses to electromagnetic fields emitted from hand-held metal detectors (HHMDs). As a point of reference, the results

are related to two voluntary international safety standards: the ICNIRP Guidelines (ICNIRP 1998a, 1998b) and the IEEE C95.1 Standard (IEEE 1991). These standards are intended to protect exposed individuals from immediate (acute) effects. These standards are also intended to protect the exposed individuals from effects due to heating or nerve stimulations. Specific information or limits for pregnant women are not given. This study does not address long-term magnetic field effects.

There are numerous non-medical sources which produce significant levels of exposure to radiofrequency and microwave radiation. The public is increasingly concerned about perceived adverse health effects from electromagnetic (EM) field-emitting devices such as mobile phones, mobile phone base stations, power lines and security devices (anti-shoplifting systems and metal detectors). Millions of pregnant women are exposed to electromagnetic fields they often do not recognize. Particularly in the case of a pregnant woman it is important to keep the exposure to the women and their foetuses below levels outlined in existing safety standards.

The ICNIRP Guidelines cover the frequency range from DC to 300 GHz, whereas the IEEE C95.1 Standard cover the range from 3 kHz to 300 GHz. For the general public and for frequencies below 100 kHz the IEEE C95.1 Standard specifies the current density as $J_{\text{rms, max}} \text{ (mA cm}^{-2}\text{)} = 15.7 \times f$ with f the frequency in MHz. Above 100 kHz, IEEE C95.1 specifies only a maximum SAR of 1.6 W kg^{-1} averaged over any 1 g of contiguous tissue. The ICNIRP standard defines the current density for the head and trunk below 100 kHz. Between 100 kHz and 10 MHz, both the maximum current density and the maximum SAR are specified. Above 10 MHz, only values for the maximum SAR are defined. For the general public, ICNIRP specifies the current density (averaged over 1 cm^2) as $J_{\text{rms, max}} \text{ (mA m}^{-2}\text{)} = f/500$ with f the frequency in Hertz. Between 100 kHz and 10 MHz, both the current density and the specific absorption rate are specified. Above 100 kHz, ICNIRP specifies the maximum SAR as 2 W kg^{-1} averaged over any 10 g of contiguous tissue. Neither the ICNIRP Guidelines nor the IEEE C95.1 Standard considers cancer, teratogenic and embryotoxic effects in the derivation of the exposure limits for SAR and induced current density.

For the induced current density, the ICNIRP Guidelines provide more restrictive limits compared to the IEEE C95.1 Standard (by a factor of 80). The main reason for this difference is the basis for the two standards. At 1 kHz, ICNIRP specifies maximum permissible current density of 2 mA m^{-2} (averaged over 1 cm^2 area) as the threshold for acute changes in the central nervous system excitability (e.g. direct nerve stimulation) for the general public and other related effects. In contrast, the IEEE C95.1 Standard specifies a maximum induced current density of 157 mA m^{-2} at 1 kHz for the general public.

Radiofrequency (RF) and microwave electromagnetic fields are known to lead to temperature increase in the human body. Most of the work on teratogenic effects of RF fields has focused on these thermal effects (Nelson 1991, Lary *et al* 1982, 1983a, 1986). A series of studies published by Lary *et al* examined the effect of thermal RF irradiation of pregnant rats on various foetal outcomes (Lary *et al* 1982, 1983b, 1986). They found that RF-induced hyperthermia in the postimplantation period caused a significant rise in foetal malformations, and a reduction in foetal weight and length. Hyperthermia during days 7 to 9 caused an increase in dead or resorbed foetuses. Exposure was associated with a significant increase in pre-implantation malformations (Lary *et al* 1982). The teratogenic and embryotoxic effects of thermal RF exposures are related to the temperature induced in the pregnant rat as well as the length of time her temperature is elevated (Lary *et al* 1983). The same publication reports a threshold temperature of $41.5 \text{ }^\circ\text{C}$ for both birth defects and prenatal death.

Gandhi and Kang (2001) used the impedance method to calculate the electric fields and induced current densities in millimetre resolution anatomic models of the human body (an

adult, a 10-year-old child and a 5-year-old child). They exposed the models to non-uniform magnetic fields typical for two representative electronic article surveillance devices at 1 kHz and 30 kHz, respectively. They compared the peak current densities with the limits given in the ICNIRP Guidelines. For both article surveillance devices, the maximum 1 cm^2 area-averaged current densities for the brain of the model of the adult were lower than the basic, induced current density limits of the ICNIRP Guidelines. However, for the model of a 10-year-old child the current density reaches the ICNIRP limit and for the model of the 5-year-old child the current density is two times higher than the ICNIRP limit.

Fleming and Joyner (1992) found that the specific absorption rate (SAR) induced in simple spheroidal models of the embryo or foetus can exceed occupational limits recommended by the International Nonionizing Radiation Committee of the International Radiation Protection Association (INIRC-IRPA), the American National Standards Institution (ANSI) and the Standards Association for Australia (SAA) for the general public, when the mother is exposed to radiofrequency radiation that is equal to the occupational exposure limits. The authors used simple symmetric geometries for the pregnant woman and assumed plane wave exposure. The prenatal exposure was estimated using the finite element method (FEM). They conclude that by applying current exposure limits, the results indicate that overexposure to the embryo or foetus can occur in early pregnancy at 80 MHz–100 MHz, and in late pregnancy from 300 MHz–1500 MHz.

2. Methods

2.1. FDTD method for quasi-static frequencies

The problem of human exposure to low frequency electromagnetic fields has been the subject of many studies and numerical simulations. Various numerical methods have been used for such simulations including FEM, integral equation (IE) methods, finite difference (FD) techniques and finite difference time domain (FDTD) methods. In all cases, these methods take advantage of the quasi-static nature of the EM fields. For quasi-static problems the dimensions of the simulation model are small in comparison to the wavelength. The relatively crude and computationally costly FDTD method has gained growing interest for quasi-static problems. This is because of its robustness, suitability to handle complex problems composed of millions of cells and general independence from electrical properties of the materials being analysed. The exponential growth of computer performance as well as various enhancements of the technique has made FDTD a popular and widely applied technique for various problems. In its classical form, the FDTD method is not a very attractive method for low frequency problems. The required simulation times may be too long for anatomical models even with moderate spatial resolution. For instance, for a problem at 1 kHz, with spatial discretization of $\Delta x = \Delta y = \Delta z = 1 \text{ cm}$, from the Courant stability criterion, the duration of one time step would be 19 ps. Allowing for six periods of the source signal, the number of time steps required for the simulation would be $N = 3 \times 10^8$. Even on a supercomputer, the simulation would run for years. To overcome this problem we used the frequency scaling method used in various publications and compared with analytic solutions by several authors (De Moerloose *et al* 1997, Furse and Gandhi 1998, Gandhi and Chen 1992, Gandhi 1995, Gustrau *et al* 1999, Potter *et al* 2000). This method overcomes excessive simulation times and has been successfully applied to low frequency dosimetry simulations. The frequency scaling method uses the quasi-static nature of the electromagnetic field. For quasi-static electromagnetic fields the imaginary part ($\omega\epsilon$) of the complex conductivity of biological tissue

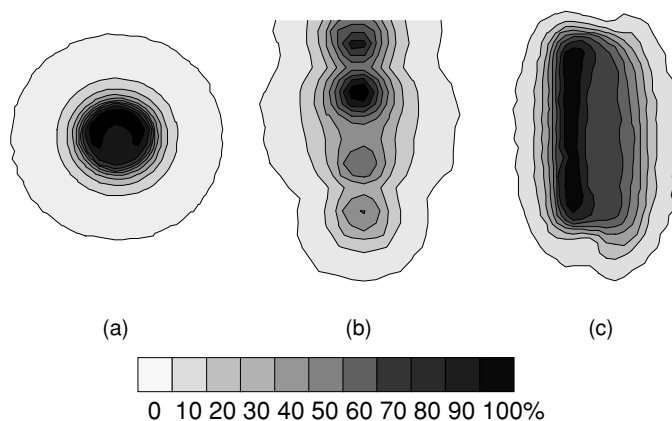


Figure 1. Field patterns of the vector magnitude of the magnetic field measured 2 cm above each of the three typical HHMDs. Each pattern is normalized to the maximum value of the individual HHMD. The maximum values are 1.7 A m^{-1} (Adams), 1.8 A m^{-1} (Omni) and 1.3 A m^{-1} (Control Screening) for the HHMD in plots a, b and c, respectively. The distribution of the magnetic field perpendicular to the loop is shown in figure 4.

is small in comparison to the real part (σ), where σ and ϵ are the electrical conductivity and the permittivity, respectively.

The actual FDTD simulation was performed at an artificially-scaled ‘higher’ frequency f' . This higher frequency has to be again a signal with quasi-static characteristics. We used the commercial FDTD software package, XFDTD Version 5.0. After the FDTD computations were performed at frequency f' , the induced electric field E' at this simulation frequency (f') was scaled to the frequency of interest (f) using (1):

$$E(f) = \frac{f}{f'} E'(f'). \quad (1)$$

Equation (1) specifies $E(f)$ as the electric field (E field) at the frequency of interest, $E'(f')$ as the E field at the higher (scaled) frequency, f as the frequency of interest and f' as the higher (scaled) frequency.

At the boundary of the calculation space, we used the perfectly matched layer (PML) conditions with 15 layers. PML conditions were used because they are superior to most standard absorbing boundary conditions.

2.2. Measurement system to map the HHMD fields

We used small magnetic field probes, consisting of three orthogonal loops, each with a 1 cm diameter loop. A three-axis, mechanical scanning system made of non-conducting materials was used together with the probes to determine the spatial and temporal characteristics of the fields emitted by nine HHMDs (Casamento 2002). For each HHMD all three components (H_x , H_y and H_z) of the magnetic field were measured in horizontal planes 1 cm, 2 cm, 5 cm and 11 cm above the HHMD. All nine HHMDs emitted sinusoidal, continuous wave (CW) fields. Data on the spatial distribution of the fields are shown in figure 1 for three typical HHMD magnetic field distributions.

Figure 2 shows the field pattern of the simulated loop (single turn loop with 8 cm in diameter) for a maximum magnetic field of 1 A m^{-1} . Figures 1(a) and 2 show good correlation of the field pattern for the simulated loop and measured HHMD. This kind of spatial distribution creates a magnetic field with the most uniform distribution over an area

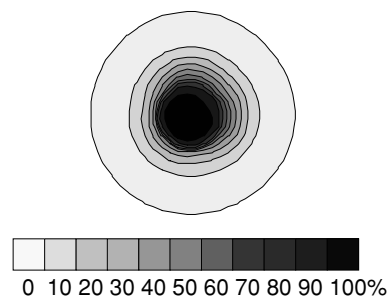


Figure 2. Field pattern 2 cm above a simulated HHMD. The maximum vector magnitude of the magnetic field is 1 A m^{-1} . The distribution of the magnetic field perpendicular to the loop is shown in figure 4.

Table 1. Properties of the three tissues assumed for the calculations.

Tissue	Conductivity σ (S m^{-1})	Density ρ (kg m^{-3})
Muscle	0.7	1059
Skin/Fat	0.18	1034
Foetus	0.6	1000

and concentrates the field in this region. The concentration of the field in a limited area causes the highest local current density and SAR in the abdomen of the pregnant woman. To address worst-case assumptions all HHMDs were modelled as a single loop with a diameter of 8 cm.

2.3. Model of a pregnant woman exposed to HHMDs

Data were obtained that described the shape of the body surface of a pregnant woman in the 34th week of pregnancy. This data was provided by FarField Technology Limited, Christchurch, New Zealand. Then the output CAD file (Computer Aided Design) was voxelized with a resolution of 10 mm. The total FDTD calculation space was 269 360 voxels ($56 \times 65 \times 74$ voxels) including 7 voxels of free space to the absorbing boundary layer. Due to the lack of an internal anatomical dataset of a pregnant woman, we decided to develop a semi-heterogeneous computer model of a pregnant woman and foetus based on the available laser scanned data described above. The model used for this paper consisted of three different types of tissue shown in Table 1: 'Muscle', 'Skin/Fat' and the 'Foetus'.

The model was converted from a surface model to a volume model as follows. Internal voxels were assigned the electrical properties of muscle tissue. The electrical properties of all surface voxels were given a value of the mean value of skin and fat. The foetus was modelled as a sphere, 20 cm in diameter, located 1 cm below the model surface. It was assigned a value of electrical properties that were the mean of those of muscle, uterus and blood.

For quasi-static applications the imaginary part of the complex conductivity ($\omega\epsilon$), is small compared to the real part (σ). Therefore, the permittivities ϵ_r of all tissues are irrelevant for the calculation and were set to 1.0. This leads to a faster propagation of the electromagnetic waves through the model and therefore to a reduced simulation time (Gandhi and Chen 1992). The conductivity values were taken from Gabriel *et al* (1996c). In order to establish worst-case conditions, the conductivity values selected were those that exist in tissues of interest at the highest exposure frequency (1.8 MHz) and at the upper limit of the uncertainty interval for the conductivity given by Gabriel *et al* (1996a, 1996b, 1996c, 1996d). All other calculations

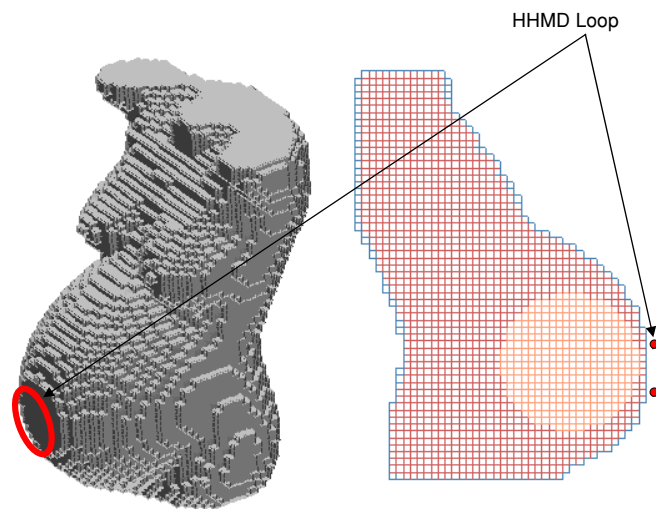


Figure 3. 3D representation and a vertical cut through the pregnant woman model and the HHMD modelled as a loop with 8 cm in diameter 1 cm away from the surface of the model.

at lower frequencies were performed with this electrical conductivity representing the tissue at 1.8 MHz.

The HHMD was modelled as a single loop with a diameter of 8 cm positioned in front of the abdomen 1 cm away from the surface of the model (figure 3).

Finally, computations were performed to calculate the induced current density and the specific absorption rate. The results are presented below.

3. Results

3.1. Current density and SAR

The calculations were performed at 10 MHz and scaled to the frequency of interest using equation (1). The highest 1 cm^2 area-averaged current density was found in the second layer which corresponds to a depth of 1 cm. To relate the calculated internal fields to the emitted magnetic fields of the actual HHMD, the current density and the SAR were linearly scaled to the actual magnetic field at a distance of 2 cm from the HHMD. The field distribution was measured as described in section 2.2 for nine different HHMDs at four distances: 1 cm, 2 cm, 5 cm and 11 cm, away from the outer surface of the HHMD. Figure 4 shows the results of the computer-modelled approximation of the HHMD as a single-turn-loop 8 cm in diameter. Comparison with measured values from a typical HHMD led to similar maxima of the magnetic fields versus distance from the HHMD.

In the pregnant woman model, the highest current density averaged over a 1 cm^2 area was found 1 cm below the surface of the body. It is located in the area where the conductivity rises from 0.18 S m^{-1} (skin/fat) to 0.7 S m^{-1} (muscle). All maximum values for current density and SAR are located in one plane. This plane of maximum field values is located 1 cm below the model surface and 2 cm apart from, and parallel to, the HHMD loop. The shape of the current density distribution was circular with the same diameter (8 cm) as the HHMD model and dropped off rapidly with increasing depth into the human model. Figure 5 shows the current density distribution in the sagittal plane, bisecting the centre of the model.

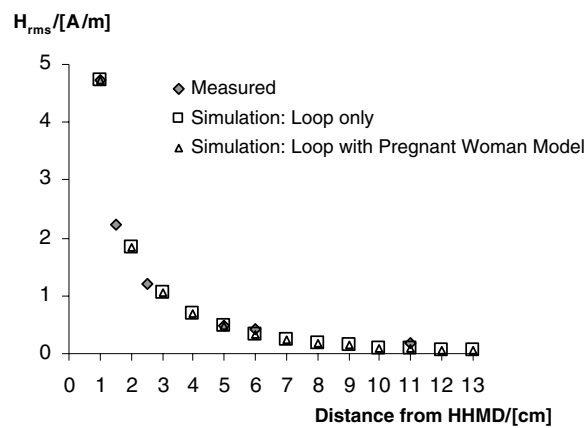


Figure 4. Measured and calculated maximum values of the magnetic field versus distance from the HHMD in air. Plots show (i) measured fields from HHMDs illustrated in figure 1, (ii) computed fields in air versus distance from an 8 cm diameter loop model, and (iii) computed fields versus distance from the simulated loop when the loop is positioned 1 cm away from the pregnant woman model.

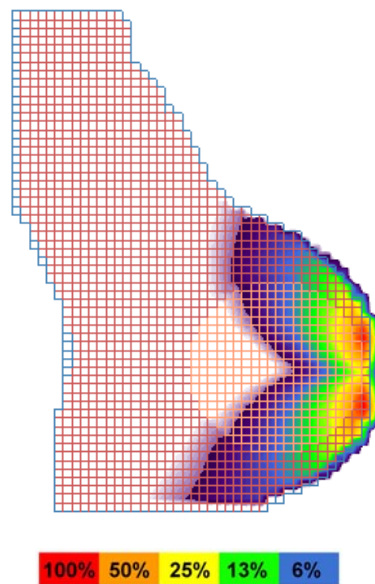


Figure 5. Current density (J) distribution averaged over 1 cm^2 in the centre plane through the pregnant woman model (maximum value of $J = 29 \text{ mA cm}^{-2}$ for a loop producing 1 A m^{-1} at the surface of the body).

Table 2 summarizes the maximum current density (averaged over a 1 cm^2 area) and the SAR (averaged over $1 \text{ cm}^3 = 1 \text{ g}$) calculated for nine different HHMD. These values were compared to the recommended limits outlined by the ICNIRP Guidelines and the IEEE C95.1 Standard. We related the results of our computations to the respective maximum permissible induced current density and SAR in these standards as follows. The ratio between the maximum permissible value in the ICNIRP Guidelines or IEEE C95.1 Standard and the maximum value of current density found in our model was defined as the current density safety

Table 2. Maximum magnetic field (H_{rms}), induced current density 1 cm² area-averaged (J_{rms}), specific absorption rate (SAR) and the safety factors for the induced current density (SF- J) and the specific absorption rate (SF-SAR) in relation to the ICNIRP Guidelines and the IEEE C95.1 Standard.

HHMD	f (kHz)	H_{rms}		J_{rms}		SF- J		SAR	SF-SAR	
		(A m ⁻¹)	(mA m ⁻²)	ICNIRP (1)	C95.1 (1)	(μ W kg ⁻¹)	ICNIRP (10 ³)	C95.1 (10 ³)		
Schiebel	7.9	1.6	1.7	9	742	0.003	–	–	–	–
Ranger	13.3	4.8	8.3	3	252	0.06	–	–	–	–
Adams	20.8	1.7	2.6	16	1236	0.007	–	–	–	–
Metorex	23.6	1.9	5.8	8	643	0.03	–	–	–	–
CEIA	45.8	2.1	12.6	7	571	0.15	–	–	–	–
Garrett	95.0	2.9	35.7	5	418	1.2	–	–	–	–
Omni	132.0	1.8	17.3	15	–	0.3	7131	5705	–	–
MetalTec–Torfino	267.7	0.5	8.9	60	–	0.07	26919	21535	–	–
ControlScreening	1807	1.3	167.8	22	–	26.5	75	60	–	–

Table 3. Maximum current density J in 1 cm depth calculated at 1 MHz for 1 A m⁻¹ at 2 cm distance from the HHMD with the method of frequency scaling and directly.

	Current density J (mA m ⁻²)	Current density J normalized (1)
Directly calculated at 1 MHz	28.59	1
Scaled from 10 MHz	28.88	1.01

factor (SF- J). The ratio between the maximum permissible value in the ICNIRP Guidelines or IEEE C95.1 Standard and the maximum value of SAR found in our model and was defined as the SAR safety factor (SF-SAR).

3.2. Validation of the frequency scaling method

To prove our implementation of the scaling method with XFDTD, we ran a simulation at 1 MHz without scaling and compared the results with scaled computations. The same geometry described above was used. At a frequency of 1 MHz, without scaling, it took 6 days on a Pentium 4, 1.5 GHz PC to solve the problem. Then we used the scaling technique to solve the problem at 10 MHz and scaled the results to 1 MHz. The scaled computation took 14 h.

Table 3 shows excellent agreement between the directly calculated current density in 1 cm depth for field strengths of 1 A m⁻¹ at a distance of 2 cm away from the HHMD and the scaled values calculated at 10 MHz. This proved the FDTD scaling method to be a powerful and accurate tool for low frequency dosimetry calculations.

3.3. Comparison with analytic results

The FDTD results were compared with an analytical solution of induced currents in an ellipsoid exposed by a homogeneous transversal magnetic field outlined by Baraton and Hutzler (1995). The analytical formula for the absolute value of the current density inside an ellipsoid exposed to a homogeneous magnetic field is given by (2), with the polar coordinates radius r and the elevation angle θ . β is the ratio between the semi-minor axis a and the semi-major axis b of the ellipsoid

$$J(r, \theta) = \frac{2\pi f \sigma \mu H r}{1 + \beta^2} \sqrt{\sin^2 \theta + \beta^2 \cos^2 \theta}. \quad (2)$$

We calculated the maximum current density J in 1 cm depth at 1 MHz for 1 A m^{-1} at 2 cm distance from the HHMD at the maxima of (2) which are at $(r = a, \theta = \pi)$ and $(r = b, \theta = 0)$. Because the magnetic field of the loop is highly non-uniform we assumed a small ellipsoid with $a = 0.5 \text{ cm}$ and $b = 4 \text{ cm}$. This small ellipsoid covers a volume in which the magnetic field of the loop is approximately homogeneous. The conductivity of the ellipsoid was assumed to be $\sigma = 0.7 \text{ S m}^{-1}$ which corresponds to the conductivity in 1 cm depth. At both maxima, the analytically calculated current density has the same value of 27.2 mA m^{-2} which is close to the FDTD result for the maximum current density of 28.6 mA m^{-2} . Based on the simple approximation for the analytical solution the 5% deviation between the FDTD result and the analytic solution can be seen to be in excellent agreement.

4. Conclusions

The highest current density found in our model is 8.3 mA m^{-2} and the highest SAR is $26.5 \mu\text{W kg}^{-1}$. We compared the results of our computations to the recommended limits for the general public. These recommended limits are specified in both the ICNIRP Guidelines and the IEEE C95.1 Standard. We defined the ratio between the maximum permissible value by both standards and the maximum values found in our model as the current-density safety factor (SF- J) and the SAR safety factor (SF-SAR). Compared to the recommended limits for the induced current density outlined by the ICNIRP Guidelines, a minimum safety factor of 3 exists. Compared to the IEEE C95.1 Standard, a safety factor of 60 000 for the specific absorption rate was found. Neither standard provides specific information or exposure limits for pregnant women or their foetuses. The ICNIRP Guidelines provide some information on direct effects of electric and magnetic fields on reproductive outcome based on epidemiological studies. The IEEE C95.1 Standard includes pregnant women and their foetuses in an 'uncontrolled environment'. Here, individuals have no knowledge or control of their exposure.

The very low SAR values are several orders of magnitude below the IEEE limits, and even lower for the ICNIRP Guidelines. In addition, applying the 6 min averaging rule for the SAR would increase the safety factors by 10–100. Only the IEEE C95.1 Standard specifies a time averaging for the induced current density of 1 s. Since usual HHMD exposure lasts longer than 1 s, an averaging of the calculated values is not necessary.

None of the HHMDs violates the recommended limits of the ICNIRP Guidelines or the IEEE C95.1 Standard regarding the induced current density and the SAR. The lowest safety factor of 3 for the induced current density was found for the Ranger HHMD which emitted a 13 kHz magnetic field. The lowest SAR safety factor of 60 000 was found for the HHMD from Control Screening which operated at 1.8 MHz. Based on the very low SAR (in the $\mu\text{W kg}^{-1}$ range) and an induced current density below the recommended exposure limits, no significant and/or measurable temperature rise or nerve stimulation will occur in a pregnant woman or her foetus from the HHMDs studied.

Acknowledgments

The authors would like to thank Giorgi Bit-Babik, PhD from the Motorola Corporate EME Research Lab for assistance in manipulating the pregnant woman model data. In addition, we would like to thank the Federal Aviation Administration for supporting this project and FarField Technology for providing the CAD data for the pregnant woman model.

References

- Baraton P and Hutzler B 1995 Magnetically induced currents in the human body *IEC Technology Trend Assessment*
- Casamento J 2002 Comparison of magnetic fields emitted from security screening devices with magnetic field immunity standards *IEEE Int. Symp. on Electromagnetic Compatibility—Proc.* pp 937–40
- CENELEC TC 106X 2001 Evaluation of human exposure to electromagnetic fields from devices used in electronic article surveillance (EAS), radio frequency identification (RFID) and similar applications *European Committee for Electrotechnical Standardization* (Brussels: EC) European Standard—EN 50357
- De Moerloose J, Dawson T W and Stuchly M A 1997 Application of the finite difference time domain algorithm to quasi-static field analysis *Radio Science* **32** 329–41
- Fleming A H and Joyner K H 1992 Estimates of absorption of radiofrequency radiation by the embryo and the fetus during pregnancy *Health Phys.* **63** 149–59
- Furse C and Gandhi O P 1998 Calculation of electric fields and currents induced in a millimeter-resolution human model at 60 Hz using the FDTD method *Bioelectromagnetics* **19** 293–9
- Gabriel C 1996a Compilation of the dielectric properties of body tissues at RF and microwave frequencies *Report AL/OE-TR-1996-0037*, Armstrong Laboratory (AFMC), Radiofrequency Radiation Division, Brooks AFB, TX
- Gabriel C, Gabriel S and Corthout E 1996b The dielectric properties of biological tissues: I. Literature survey *Phys. Med. Biol.* **41** 2231–49
- Gabriel S, Lau R W and Gabriel C 1996c The dielectric properties of biological tissues: II. Measurements in the frequency range 10 Hz to 20 GHz *Phys. Med. Biol.* **41** 2251–69
- Gabriel S, Lau R W and Gabriel C 1996d The dielectric properties of biological tissues: III. Parametric models for the frequency spectrum of tissues *Phys. Med. Biol.* **41** 2271–93
- Gandhi O P 1995 Some numerical methods for dosimetry: extremely low frequencies to microwave frequencies *Radio Science* **30** 161–77
- Gandhi O P and Chen J Y 1992 Numerical dosimetry at power-line frequencies using anatomically based models *Bioelectromagnetics* (Suppl 1) 43–60
- Gandhi O P and Kang G 2001 Calculation of induced current densities for humans by magnetic fields from electronic article surveillance devices *Phys. Med. Biol.* **46** 2759–71
- Gustrau F, Bahr A, Rittweger M, Goltz S and Eggert S 1999 Simulation of induced current densities in the human body at industrial induction heating frequencies *IEEE Trans. Electromagn. Compat.* **44** 480–6
- Institute of Electrical and Electronics Engineers (IEEE) SCC28 1991 *IEEE Standard for Safety Levels With Respect to Human Exposure to Radiofrequency Electromagnetic Fields, 3 kHz to 300 GHz* (New York: IEEE) C95.1–1991
- International Commission on Non-Ionizing Radiation Protection (ICNIRP) 1998a Guidelines for limiting exposure to time-varying electric, magnetic, and electromagnetic fields (up to 300 GHz) *Health Phys.* **74** 494–522
- International Commission on Non-Ionizing Radiation Protection (ICNIRP) 1998b Response to questions and comments on ICNIRP *Health Phys.* **75** 438
- Lary J M, Conover D L, Foley E D and Hanser P L 1982 Teratogenic effects of 27.12 MHz radiofrequency radiation in rats *Teratology* **26** 299–309
- Lary J M, Conover D L, Johnson P H and Burg J R 1983a Teratogenicity of 27.12 MHz radiation in rats in relation to duration of hyperthermic exposure *Bioelectromagnetics* **4** 249–55
- Lary J M, Conover D L and Johnson P H 1983b Absence of embryotoxic effects from low-level (nonthermal) exposure of rats to 100 MHz radiofrequency radiation *Scand. J. Work Environ. Health* **9** 120–7
- Lary J M, Conover D L, Johnson P H and Hornung R W 1986 Dose-response relationship between body temperature and birth defects in radiofrequency-irradiated rats *Bioelectromagnetics* **2** 141–9
- Nelson B K, Conover D L, Krieg E F, Snyder D L and Edwards R M 1997 Interactions of radiofrequency radiation-induced hyperthermia and 2-methoxyethanol teratogenicity in rats *Bioelectromagnetics* **18** 349–59
- Potter M E, Okoniewski M and Stuchly M A 2000 Low frequency finite difference time domain (FDTD) for modeling of induced fields in humans close to line sources *J. Comput. Phys.* **162** 82–103